Analytical Model for Calculating the Radiation Field of Microstrip Antennas With Artificial Magnetic Superstrates: Theory and Experiment

Hussein Attia, *Student Member, IEEE*, Leila Yousefi, *Member, IEEE*, and Omar M. Ramahi, *Fellow, IEEE*

***Abstract*—A fast analytical solution for the radiation field of a microstrip antenna loaded with a generalized superstrate is proposed using the cavity model of microstrip antennas in conjunction with the reciprocity theorem and the transmission line analogy. The proposed analytical formulation for the antenna's far-field is much faster when compared to full-wave numerical methods. It only needs 2% of the time acquired by full-wave analysis. Therefore the proposed method can be used for design and optimization purposes. The method is verified using both numerical and experimental results. This verification is done for both conventional dielectric superstrates, and also for artificial superstrates. The analytical formulation introduced here can be extended for the case of a patch antenna embedded in a multilayered artificial dielectric structure. Arguably, the proposed analytical technique is applied for the first time for the case of a practical microstrip patch antenna working in the Universal Mobile Telecommunications System (UMTS) band and covered with a superstrate made of an artificial periodic metamaterial with dispersive permeability and permittivity.**

***Index Terms*—Artificial magnetic superstrate, cavity model, metamaterials, microstrip antennas, split ring resonators.**

I. Introduction

THE addition of a superstrate layer over microstrip patch antenna (MPA) has been reported to allow for the enhancement of the antenna gain and radiation efficiency [1]–[8]. Furthermore, superstrate layers are often used to protect the MPA from its environment hazards, especially when placed on aircrafts and missiles. Earlier publications were focused on understanding how the superstrate affects the resonant frequency and subsequent power matching concerns [9]. While the gain of MPAs can be increased by using planar arrays; a solution mostly attractive because it does not change the vertical profile of the antenna structure, arrays, however, need a feeding network which introduces losses and design complications [10].

Several configurations of superstrates were used to improve antenna radiation properties, such as dielectric slabs [11], [12], electromagnetic bandgap (EBG) structures [13], [14], highly-reflective surfaces [8], and the most recently artificial magnetic superstrates [7], [15].

Using magneto-dielectric materials with high *positive* permeability and permittivity values as the superstrate of MPA decreases the wavelength in the media, leading to a lower profile of the whole structure [2], [7]. In [16], the potential application of magneto-dielectric materials as a superstrate to improve the gain of MPA was investigated without considering physical realization of the artificial superstrate. Latrach *et al.* [17] used edge-coupled split ring resonator (SRR) inclusions to provide artificial superstrate comprising alternately layers with negative permeability and positive index of refraction materials to increase the gain of patch antenna. In [7], an artificial magnetic material based on the broadside-coupled split ring resonator SRR inclusions was used as a superstrate for a MPA to increase the antenna gain and radiation efficiency.

To analyze the composite structure (antenna with superstrate), full-wave electromagnetic simulation tools which utilize numerical methods are usually used. However, using numerical methods to analyze metamaterials, or periodic structures in general, is an expensive computational task which requires considerable computer resources. The primary reason for such large computational burden is the resolution needed to capture the quasi-static resonance behavior in the metamaterial particles which are electrically very small. Therefore, numerical methods may not be practical for real-world designs that require several runs for optimization. Developing a fast analytical method to analyze such structures, which is the focus of this paper, can accelerate the design process, and also provides optimization opportunities.

So far several analytical methods for calculating the far-field of Hertzian dipole in multi-layer structure, has been reported in literature [1]–[6] and [18], [19]. In [1], Green's function and the stationary phase integration approach were used to calculate the gain of an infinitesimal dipole embedded in the top layer of a two-layer dielectric structure. Additionally, in [1], it was shown that a resonance condition may be created, whereby gain and radiation resistance are improved over a significant bandwidth. Later in [2], the reciprocity theorem and transmission line (TL) analogy were used to provide asymptotic formulas for gain and beamwidth of a Hertzian dipole embedded within a grounded substrate and covered with a superstrate. In [18], [19], the TL analogy method was used to compute the radiation patterns of arbitrarily directed simple dipole source that is embedded in a multilayered dielectric structure. Also, a dielectric resonator

Manuscript received May 02, 2010; revised September 09, 2010; accepted October 26, 2010. Date of publication March 03, 2011; date of current version May 04, 2011. This work was supported in part by the Ministry of Higher Education, Egypt, Research in Motion (RIM) Inc., and in part by the Natural Sciences and Engineering Research Council (NSERC) of Canada under the NSERC/RIM Industrial Research Associate Chair and Discovery Programs.

The authors are with the Electrical and Computer Engineering Department, University of Waterloo, Waterloo, ON N2L 3G1 Canada (e-mail: h2attia@uwaterloo.ca; lyousefi@uwaterloo.ca; oramahi@ece.uwaterloo.ca).

Color versions of one or more of the figures in this paper are available online at http://ieeexplore.ieee.org.

Digital Object Identifier 10.1109/TAP.2011.2122295

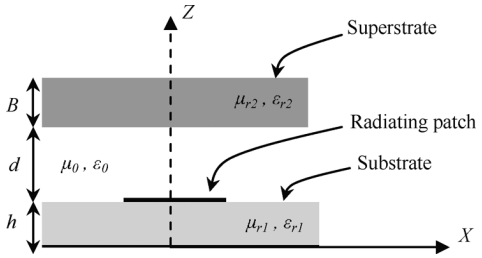

Fig. 1. Microstrip patch antenna covered by a superstrate.

antenna covered with plain dielectric superstrate was analyzed [18]. The straightforward method proposed in this work based on the cavity model avoids the need to use the particle swarm optimization (PSO) method used in [18] to obtain a set of Hertzian dipoles representing the antenna to be analyzed using the reciprocity theorem and TL analogy.

Although several attempts have been reported to develop analytical methods, most of those works consider the case of a simple infinitesimal dipole antenna covered with plain dielectric superstrate [1]–[6] and [18], [19]. In this paper, we consider a practical microstrip patch antenna working in the UMTS band and covered with an artificial magnetic (metamaterial) superstrate used for increasing the antenna directivity. The cavity model of a MPA in conjunction with the reciprocity theorem and the transmission line analogy is used to develop a fast analytical solution for the radiation field. The artificial superstrate constituted by split ring resonators SRR printed on both sides of a dielectric slab is characterized analytically by obtaining its effective permeability and permittivity.

The organization of this paper is as follows: in Section II, the radiation patterns of a MPA covered with a generalized superstrate layer at some distance in free space are calculated by replacing the MPA with two magnetic current sources based on the cavity model and then using reciprocity theorem and the TL analogy to compute the antenna directivity. In Section III, the proposed analytical formulation is verified through a comparison with numerical full wave simulation results, where the directivity of a MPA covered with different conventional superstrates is calculated. Section IV shows the application of the analytical technique to a MPA loaded with an artificial magnetic superstrate to enhance the directivity of the MPA, experimental results are used to validate the analytical formulation. Finally, summary and conclusion are provided in Section V.

II. Analytical Formulation of the Antenna's Far-Field

The basic problem to be studied is shown in Fig. 1. A MPA is covered with a superstrate layer at a distance d in free space. The MPA is printed on a grounded substrate of thickness h having relative permeability and permittivity of μ_{r1} and ϵ_{r1}, respectively. At distance d from the substrate is the superstrate layer of thickness B having relative permeability and permittivity of μ_{r2} and ϵ_{r2}, respectively. To compute the far-field, first the MPA is modeled as a dielectric-loaded cavity [20] and then the reciprocity theorem and the transmission line analogy are applied to the whole structure (the antenna with the superstrate).

A. Reciprocity Theorem

Assume $\mathbf{J}_1, \mathbf{M}_1$ and $\mathbf{J}_2, \mathbf{M}_2$ are two groups of sources radiating inside the same medium generating the fields $\mathbf{E}_1, \mathbf{H}_1$, and $\mathbf{E}_2, \mathbf{H}_2$, respectively. The sources and fields satisfy the *Lorentz Reciprocity Theorem* in integral form [21], the formula is repeated here to make the discussion complete

$$\iint_s [\mathbf{E}_2 \times \mathbf{H}_1 - \mathbf{E}_1 \times \mathbf{H}_2]\, ds = \iiint_v [\mathbf{E}_1 \cdot \mathbf{J}_2 + \mathbf{H}_2 \cdot \mathbf{M}_1 - \mathbf{E}_2 \cdot \mathbf{J}_1 - \mathbf{H}_1 \cdot \mathbf{M}_2]\, dV. \quad (1)$$

In order to use the reciprocity theorem to compute the radiation field of MPA, one need to consider the fields ($\mathbf{E}_1, \mathbf{H}_1, \mathbf{E}_2, \mathbf{H}_2$) and the sources ($\mathbf{J}_1, \mathbf{M}_1, \mathbf{J}_2, \mathbf{M}_2$) inside a medium that is surrounded by a sphere of infinite radius. Hence, the left side of (1) is essentially zero and (1) is reduced to

$$\iiint_v [\mathbf{E}_1 \cdot \mathbf{J}_2 + \mathbf{H}_2 \cdot \mathbf{M}_1 - \mathbf{E}_2 \cdot \mathbf{J}_1 - \mathbf{H}_1 \cdot \mathbf{M}_2]\, dV = 0. \quad (2)$$

According to (2), two problems need to be established. In the first problem, the original radiating patch at $z = h$ is replaced with an electric current source $\mathbf{J}_1$ and/or a magnetic current source $\mathbf{M}_1$ (using the cavity model [20]) radiating an electric field of $\mathbf{E}_1$ and $\mathbf{H}_1$ at the observation point of $P(r, \theta, \phi)$. In the second problem, a fictitious dipole (reciprocity source) of $\mathbf{J}_2$ (choosing $\mathbf{M}_2$ is equal to zero) at the same observation point radiates a far-field of $\mathbf{E}_2$ and $\mathbf{H}_2$ at the original patch location at $z = h$. Our goal is to use (2) to formulate the far-field of the MPA as $\mathbf{E}_1$.

B. Cavity Model of Microstrip Antenna

In order to use (2) to compute the far-field of the MPA loaded with a generalized superstrate, the MPA should be replaced by a set of electric and/or magnetic current sources. The cavity model [20] of MPA to is used here to determine these equivalent currents.

The volume bound by the microstrip patch (located in the x-y plane at $z = h$) and the ground plane can be modeled as a dielectric-loaded cavity resonator by considering the top and bottom walls of this volume as perfect electric conductor (PEC) and the four side walls as ideal open circuit (magnetic walls). The mode of concern here is the dominant transverse magnetic mode (TM_{10}) which assumes a zero value of H_z but a non-zero value of E_z. By using the expression of E_z under ideal magnetic side walls boundary condition, one can formulate the equivalent magnetic current in the cavity's apertures (side walls) using the equivalence principle as $-\hat{n} \times E$. The resultant magnetic currents $\mathbf{M}_{1a}$ and $\mathbf{M}_{1b}$ will be y-directed on the two cavity's side walls parallel to the y-z plane as shown in Fig. 2. The equivalent electric current is very small (ideally zero) because $\hat{n} \times H = 0$ on the side walls. Hence, $\mathbf{J}_1$ in (2) is equal to zero.

C. Formulating the Antenna's Far-Field

According to the reciprocity theorem, a fictitious dipole (reciprocity source) of $\mathbf{J}_2$ (choosing $\mathbf{M}_2 =$ zero) at the observation

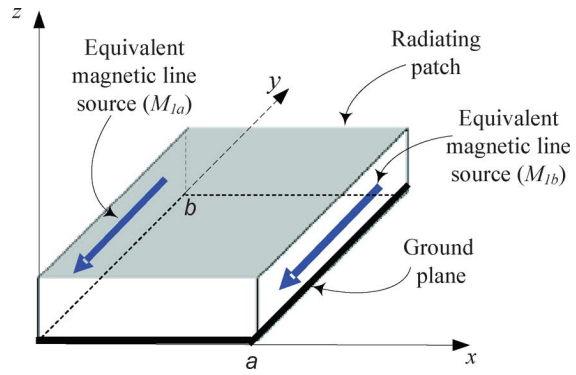

Fig. 2. Equivalent magnetic current sources representing the patch antenna.

point $P(r,\theta,\phi)$ is considered to radiate a far-field of $\mathbf{H}_2$ and $\mathbf{E}_2$ at the patch antenna location at $z = h$. Hence, (2) reduces to

$$\iiint_v [\mathbf{E}_1 \cdot \mathbf{J}_2]\, dV = -\iiint_v [\mathbf{H}_2 \cdot \mathbf{M}_1]\, dV. \tag{3}$$

The reciprocity source is assumed to have a value of $\mathbf{J}_2 = \delta(\overrightarrow{r} - \overrightarrow{r_p}) \cdot \widehat{u}$ where $\widehat{u} = \widehat{\theta}$ for TM (parallel polarization) and $\widehat{u} = \widehat{\phi}$ for TE (perpendicular polarization) incident wave on the whole structure (the patch antenna with the superstrate). Hence, (3) reduces to

$$\mathbf{E}_1(\overrightarrow{r_p}).\widehat{u} = -\iiint_v [\mathbf{H}_2 \cdot \mathbf{M}_1]\, dV. \tag{4}$$

The above equation will be used to obtain the radiation field $\mathbf{E}_{1a}$ due to one of the two equivalent magnetic current sources which can be the one at the radiation slot $x = 0$ (i.e., $\mathbf{M}_{1a}$). Then, by treating the two identical radiation slots (at $x = 0$ and $x = a$) as a two-element array, the array factor can be used to calculate the total radiated field $\mathbf{E}_1$ of the MPA covered with the superstrate, with the assumption that the existence of the superstrate does not considerably affect the current distributions in those two radiation slots.

It is observed from (4) that the $\mathbf{H}_2$ field is determined at the magnetic current source location (i.e., $\mathbf{M}_1$) due to the reciprocity source at the observation point $P(r,\theta,\phi)$ in either $\widehat{\theta}$ or $\widehat{\phi}$ direction. From the reciprocity theorem, $\mathbf{H}_2$ is proportional to the required radiation field $\mathbf{E}_1(\overrightarrow{r_p})$ due to the original patch antenna at $z = h$. The $\mathbf{H}_2$ field near the multilayered structure due to this reciprocity source is essentially a plane wave, and therefore can be found at $\mathbf{M}_{1a}$ location by modeling each layer as a transmission line segment (see Fig. 3) having a characteristic impedance and propagation constant which depend on the incident angle of θ. The propagation constants and the characteristic impedances of the multi-section transmission line equivalent model shown in Fig. 3 are derived from the oblique incidence of a plane wave on a plane interface between two dielectric regions [22] as follows:

$$\beta_1 = K_o\sqrt{\mu_{r1}\epsilon_{r1} - \sin^2(\theta)}, \quad \beta_2 = K_o\cos(\theta)$$

$$\beta_3 = K_o\sqrt{\mu_{r2}\epsilon_{r2} - \sin^2(\theta)}, \quad \beta_4 = K_o\cos(\theta).$$

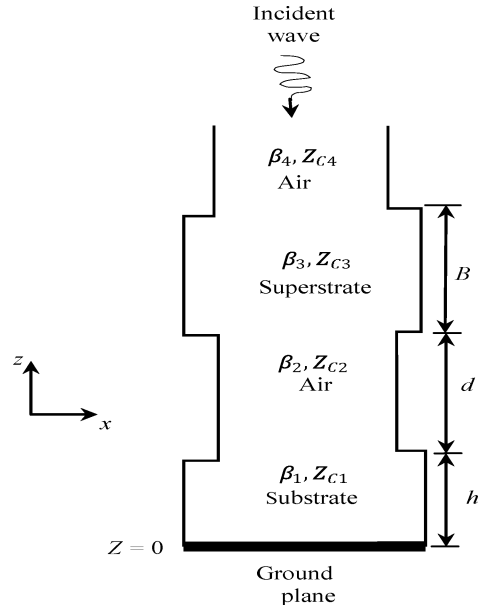

Fig. 3. Transmission line equivalent model of the structure of Fig. 1.

For TE wave or perpendicular polarization

$$Z_{c1} = \frac{\eta_o\mu_{r1}}{\sqrt{\mu_{r1}\epsilon_{r1} - \sin^2(\theta)}}, \quad Z_{c2} = \eta_o\sec(\theta)$$

$$Z_{c3} = \frac{\eta_o\mu_{r2}}{\sqrt{\mu_{r2}\epsilon_{r2} - \sin^2(\theta)}}, \quad Z_{c4} = \eta_o\sec(\theta).$$

For TM wave or parallel polarization

$$Z_{c1} = \frac{\eta_o\sqrt{\mu_{r1}\epsilon_{r1} - \sin^2(\theta)}}{\epsilon_{r1}}, \quad Z_{c2} = \eta_o\cos(\theta)$$

$$Z_{c3} = \frac{\eta_o\sqrt{\mu_{r2}\epsilon_{r2} - \sin^2(\theta)}}{\epsilon_{r2}}, \quad Z_{c4} = \eta_o\cos(\theta)$$

where, $K_o = \omega\sqrt{\mu_o\epsilon_o}$, $\eta_o = \sqrt{\mu_o/\epsilon_o}$

In case of TE incident wave ($\widehat{u} = \widehat{\phi}$) from the reciprocity source (infinitesimal dipole) located at the observation point $P(r,\theta,\phi)$ (see Fig. 4), the y component of the far-field due to this source at the location of $\mathbf{M}_{1a}$ is equal to

$$H_{2y} = \left[\frac{\jmath K_o}{4\pi}\frac{e^{-\jmath K_o r}}{r}e^{\jmath K_o(y'\sin(\theta)\sin(\phi)+z'\cos(\theta))}\right]\sin(\phi)N(\theta). \tag{5}$$

The functions $N(\theta)$ depends on θ only and it represents the current at $z = h/2$ (as midpoint in the radiation slot at $x = 0$) in the transmission line analogy (Fig. 3) due to an incident current wave of strength $\cos(\theta)$.

A straightforward method to determine the current at $z = h/2$ is to define the voltage and current on each transmission line segment shown in Fig. 3 as

$$V_i = V_i^+ e^{-\jmath\beta_i z} + V_i^- e^{\jmath\beta_i z} \tag{6}$$

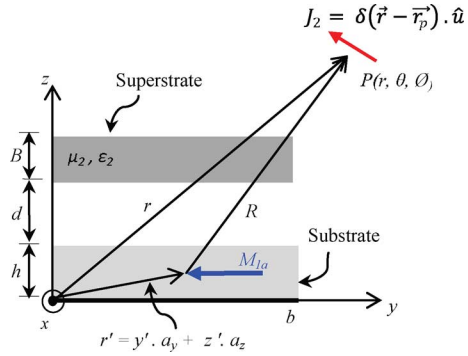

Fig. 4. Coordinate system for computing far-field from the reciprocity electric source J_2 at the patch antenna's radiation slot located at $x = 0$.

$$I_i = \frac{1}{Z_{ci}}(V_i^+ e^{-\jmath\beta_i z} - V_i^- e^{\jmath\beta_i z}) \tag{7}$$

where $i \in [1, \mathrm{N}]$ is the transmission line segment number. In the model considered here, $N = 4$. Note that as the substrate of the MPA is backed by a ground plane, $V_1^+ = -V_1^-$. Also, $V_4^+/Z_{c4} = \cos(\theta)$ for the TE case. Then, by enforcing the continuity of the voltages and current at the boundaries of these transmission line segments, one can calculate all the unknown parameters (V_i^+ and V_i^-) and hence solve for the required current at $z = h/2$. This straightforward method is extendable easily to the case of MPA covered with any number of layers.

Substituting H_{2y} from (5) in (4), the far-field $E_{1a}.\widehat{\phi}$ due to the radiation slot at $x = 0$ can be calculated. Due to the length and straightforward nature of the derivation only the final result is given here as follows:

$$E_{1a}.\widehat{\phi} = \frac{jV_oK_obe^{-\jmath K_o r}}{2\pi r} e^{\jmath(Y+Z)} \frac{\sin Y}{Y} \frac{\sin Z}{Z} \sin(\phi)\, N(\theta) \tag{8}$$

where

$$Y = \frac{K_o b}{2} \sin(\theta)\sin(\phi)$$
$$Z = \frac{K_o h}{2} \cos(\theta)$$
$$V_o = -h\, M_{1a}.$$

Note that for $h \lll \lambda$, $\sin Z/Z \cong 1$.

Similarly, the far-field due to the other radiation slot at $x = a$ can be obtained. By adding the fields due to the two radiation slots together, the total field (in ϕ direction) due to the MPA covered with the superstrate can be obtained. Another interesting way to compute the total field of the MPA in the TE mode is treating the two identical radiation slots (at $x = 0$ and a) as a two-element array. Hence, the array factor can be used to calculate the total radiated field E_ϕ of the MPA covered with the superstrate. Adopting the later method, the total field can be formulated as

$$E_\phi = \frac{jV_oK_obe^{-\jmath K_o r}}{\pi r} e^{\jmath(X+Y+Z)} \cos X \frac{\sin Y}{Y} \sin(\phi)\, N(\theta) \tag{9}$$

where

$$X = \frac{K_o\, a}{2} \sin(\theta)\cos(\phi).$$

Similarly, in the case of TM incident wave ($\widehat{u} = \widehat{\theta}$) from the reciprocity source located at the observation point $P(r, \theta, \phi)$ (see Fig. 4), the total radiated field E_θ of the MPA covered with the superstrate can be formulated as

$$E_\theta = -\frac{jV_oK_obe^{-\jmath K_o r}}{\pi r} e^{\jmath(X+Y+Z)} \cos X \frac{\sin Y}{Y} \cos(\phi)\, Q(\theta). \tag{10}$$

The functions $Q(\theta)$ depends on θ only and it represents the current at $z = h/2$ (as midpoint in the radiation slot at $x = 0$) in the transmission line analogy (Fig. 3) due to an incident current wave of strength 1 A. Hence, $V_4^+/Z_{c4} = 1$ in the transmission line equivalent model ((6) and (7)). The functions $Q(\theta)$ can be computed in the same way explained earlier in the case of $N(\theta)$.

Interestingly, the closed forms for the far-field given by (9) and (10) agree well with the ones calculated using the conventional vector potential approach [23] (see [23, Eqs (45) and (46)]) when the superstrate is air (i.e., patch antenna in free space) where $N(\theta) = \cos(\theta)$ and $Q(\theta) = 1$, this agreement verifies the proposed analytical formulation.

The far-field of the MPA covered with the superstrate is calculated at the desired frequency using (9) and (10), and integrated as follows to calculate the antenna directivity

$$Directivity(\theta, \phi) = \frac{4\pi * I}{\int_0^{2\pi}\int_0^{\pi/2} I * \sin(\theta) d\theta d\phi} \tag{11}$$

where

$$I = \cos^2(X)\frac{\sin^2(Y)}{Y^2} * (\sin^2(\phi)|N(\theta)|^2 + \cos^2(\phi)|Q(\theta)|^2).$$

III. Radiation due to a Patch Antenna Covered With Conventional Superstrate

In this section, the radiation patterns of a patch antenna covered with a conventional superstrate is investigated using the analytical technique explained in the previous section and verified using the commercial full-wave simulator HFSS.

In accordance with Fig. 1, assuming a MPA having dimensions of 36 mm × 36 mm, and printed on a substrate of Rogers RO4350 having a relative permittivity of 3.48, loss tangent of $\tan\delta = 0.004$ and a thickness of 0.762 mm. The patch is covered with a superstrate of thickness 6.286 mm. The spacing between the antenna and the superstrate is 12 mm. The three-layer radiating system is infinitely extended in the x-y plane to comply with the transmission line analogy in order to calculate the current at the patch location due to the TE and TM incident plane waves.

Three superstrates with different values of permeability and permittivity are studied here as shown in Fig. 5 for ($\mu_{r2} = 1$, $\epsilon_{r2} = 1$), Fig. 6 for ($\mu_{r2} = 16, \epsilon_{r2} = 1$), and Fig. 7 for ($\mu_{r2} = 1$, $\epsilon_{r2} = 6$). It is observed that the resultant E-plane ($\phi = 0^o$) and

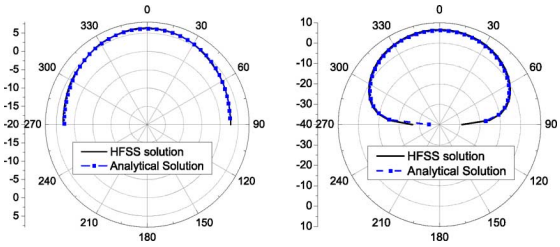

Fig. 5. The directivity radiation pattern at 2.2 GHz of the patch antenna covered with a superstrate ($\mu_{r2} = 1$ and $\epsilon_{r2} = 1$) at $d = 12$ mm, $B = 6.286$ mm and $h = 0.762$ mm. (a) E-plan and (b) H-plan.

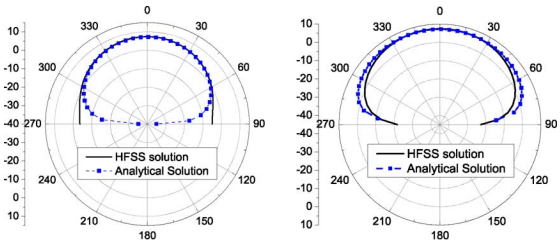

Fig. 6. The directivity radiation pattern at 2.2 GHz of the patch antenna covered with a superstrate ($\mu_{r2} = 16$ and $\epsilon_{r2} = 1$) at $d = 12$ mm, $B = 6.286$ mm and $h = 0.762$ mm. (a) E-plan and (b) H-plan.

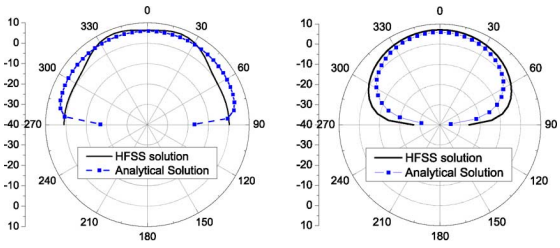

Fig. 7. The directivity radiation pattern at 2.2 GHz of the patch antenna covered with a superstrate ($\mu_{r2} = 1$ and $\epsilon_{r2} = 6$) at $d = 12$ mm, $B = 6.286$ mm and $h = 0.762$ mm. (a) E-plan and (b) H-plan.

H-plane ($\phi = 90^o$) directivity radiation patterns agree well with HFSS results in the three cases.

Fig. 8 shows a comparison between the analytically and numerically (HFSS) calculated directivity in broadside direction ($\phi = \theta = 0^o$) at 2.2 GHz of the patch antenna covered with a superstrate having a relative permeability μ_{r2} of 1 and varying relative permittivity ϵ_{r2}. Good agreement is observed between the two methods.

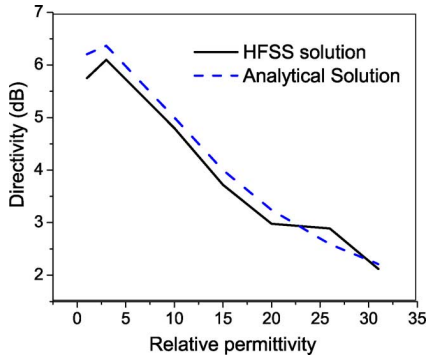

Fig. 8. The directivity of MPA shown in Fig. 1 versus the relative permittivity of the superstrate with $\mu_{r2} = 1$ at 2.2 GHz, $d = 12$ mm, $B = 6.286$ mm and $h = 0.762$ mm.

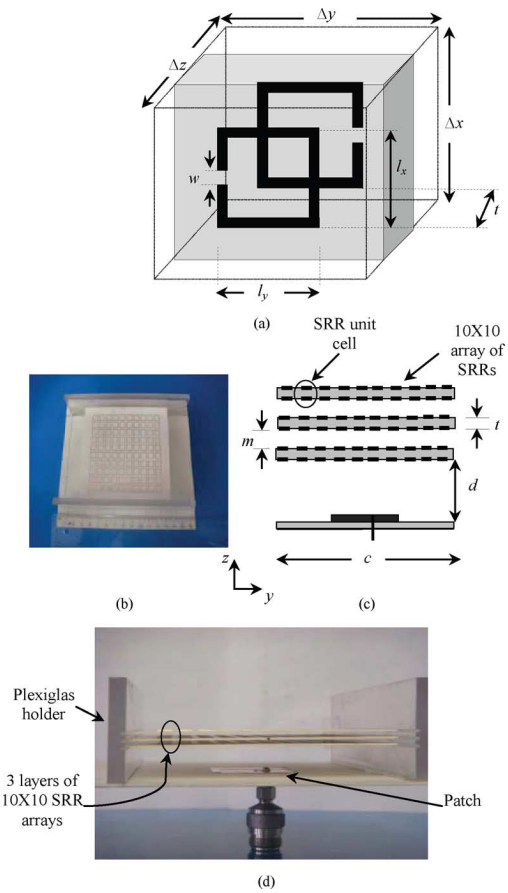

Fig. 9. Geometry of a patch antenna covered with an engineered magnetic superstrate. (a) SRR unit cell. (b) Photograph of top view. (c) Side view. (d) Experimental prototype ($t = 0.762$ mm, $m = 2$ mm, $c = 85$ mm and $d = 12$ mm).

IV. Artificial Magnetic Structure as a Superstrate for Planar Antennas

The proposed analytical solution is used here to analyze a MPA loaded with an artificial magnetic superstrate (see Fig. 9). Fig. 9(a) illustrates a broadside coupled split-ring resonator (SRR) unit cell acting as a building block of the artificial magnetic superstrate [7], [24]. The SRR inclusion consists of two parallel broken square loops. The host dielectric is made of Rogers RO4350 with a thickness of 0.762 mm, relative permittivity of $\epsilon_r = 3.48$, and loss tangent of $\tan\delta = 0.004$. A planar 10×10 array of SRRs is printed on the host dielectric layer to provide the engineered magnetic material. The superstrate used here consists of 3 layers of printed magnetic inclusions. The layers are separated by 2 mm of air layers (see Fig. 9(c)).

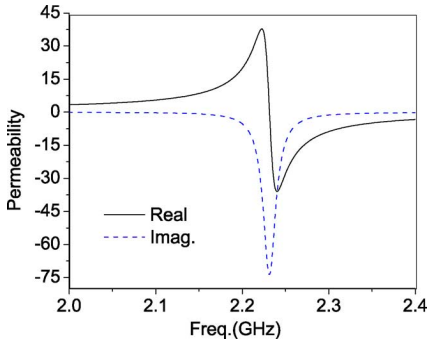

Fig. 10. Analytically calculated relative permeability of the SRR inclusions.

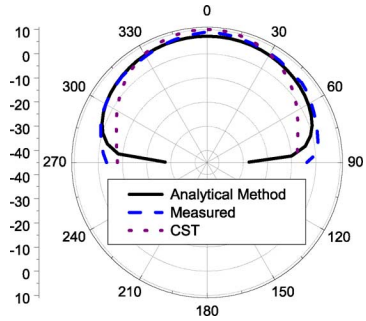

Fig. 11. The E-plane directivity radiation pattern at 2.12 GHz of the patch antenna covered with the engineered magnetic superstrate.

The SRR unit cell is analytically modeled by obtaining its effective relative permeability as

$$\mu_{r_{eff}} = 1 - \frac{\jmath\,\omega\,L_{eff}\,S}{\Delta x \Delta z \left(R_{eff} - \frac{\jmath}{\omega C_{eff}} + \jmath\,\omega\,L_{eff}\right)} \tag{12}$$

where S is the surface area of the inclusion $(l_x \times l_y)$, Δx and Δz are the unit cell sizes in x and z directions as shown in Fig. 9(a). The dimensions of the designed SRR unit cell are $\Delta x = \Delta y = 8.5$ mm, $\Delta z = 2.762$ mm, $l_x = l_y = 6.5$ mm, $w = 0.3$ mm. The width of metallic strips (s) is equal to 0.3 mm, and the metallic strips are assumed to be made of copper. Formulas for R_{eff}, C_{eff} and L_{eff} can be found in [24].

Since the SRRs are aligned in the x-y plane, the resultant effective enhanced permeability is provided only in the z direction [7]. Hence, the engineered material composed of the SRR inclusions will experience the anisotropic permeability tensor of

$$\mu = \mu_0 \begin{pmatrix} 1 & 0 & 0 \\ 0 & 1 & 0 \\ 0 & 0 & \mu_{r_{eff}} \end{pmatrix}. \tag{13}$$

The analytically calculated effective relative permeability is shown in Fig. 10.

An effective x and y-directed permittivity is provided by the stored electrical energy in the inter-cell capacitors formed in the gap regions between the metallic SRRs inclusions. In case of a z-directed electric field, the metamaterials superstrate will experience an effective permittivity equal to that of its host dielectric as the electric field would be perpendicular to the plane of the unit cell. Therefore, the artificial magnetic material composed of the SRRs inclusions will experience anisotropic electric permittivity of [25]

$$\epsilon = \epsilon_0 \begin{pmatrix} \epsilon_{r_{eff}} & 0 & 0 \\ 0 & \epsilon_{r_{eff}} & 0 \\ 0 & 0 & \epsilon_{r_{diel}} \end{pmatrix} \tag{14}$$

where

$$\epsilon_{r_{eff}} = \epsilon_{r_{diel}} \left[1 + \frac{\Delta z\, l_x}{\Delta x\, \Delta y} \frac{K(\sqrt{1-g^2})}{K(g)}\right]$$

$$g = \frac{\frac{s}{2}}{\frac{s}{2} + w}, \quad K(g) = \int_0^{\pi/2} \frac{d\theta}{\sqrt{1 - g^2\,\sin^2\theta}}.$$

According to the above formulas, the effective relative permittivity of the designed structure in the x and y directions would be equal to 5.62. Substituting the value of permittivity and permeability from (12) and (14) in the equations presented in Section II, the electric field of the MPA is calculated at the desired frequency using (9) and (10) and then integrated to calculate the antenna directivity using (11).

To verify the analytical solution of the far-field, the patch antenna covered with the SRR based artificial magnetic superstrate (see Fig. 9) has been fabricated, simulated using CST, and measured. The reason for using CST in this case is that the time domain simulation module in CST stimulates the structure using a broadband signal, broadband stimulation calculates the S-parameters for the entire desired frequency range and the radiation patterns at various desired frequencies from only one calculation run. On the other hand, frequency domain solvers such as HFSS perform a new simulation run for each frequency sample. Hence, the relationship between calculation time and frequency steps is linear unless special methods are applied to accelerate subsequent frequency domain solver runs. Therefore, the time domain solver usually is fastest when a large number of frequency samples need to be calculated.

The analytical results are compared to the numerical and experimental results for a MPA having dimensions of 36 mm × 36 mm, and is printed on a substrate of Rogers RO4350 having a relative permittivity of 3.48, loss tangent of $\tan\delta = 0.004$ and a thickness of 0.762 mm. The antenna is designed to operate at the frequency band of 2190–2210 MHz (UMTS) at which the magnetic superstrate has an effective permeability of about 15 (real part) and a magnetic loss tangent of 0.11 (see Fig. 10).

Fig. 11 shows a comparison between the analytical, numerical and experimental results of the E-plane directivity radiation pattern at the antenna's resonance frequency of 2.12 GHz, a good agreement is observed between the three methods. The H-plane directivity radiation pattern of the same structure is shown in Fig. 12, where the discrepancy in the measured results is believed to be due to the finite size of the superstrate used here. These measurement results show that the antenna directivity equals to 9.6 dB (in the broadside direction) after using the artificial magnetic superstrate compared to 6.2 dB of the patch antenna only (see Fig. 5).

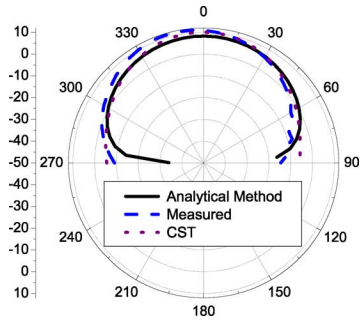

Fig. 12. The H-plane directivity radiation pattern at 2.12 GHz of the patch antenna covered with the engineered magnetic superstrate.

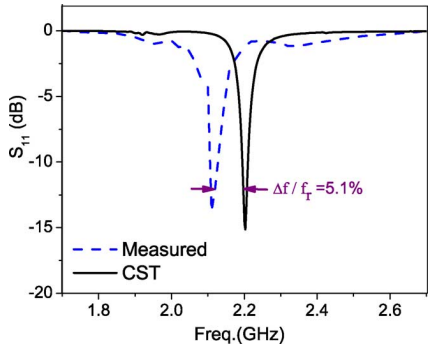

Fig. 13. The return loss of the microstrip antenna covered with the artificial magnetic superstrate.

Fig. 13 shows the reflection coefficient in dB of the microstrip antenna with the artificial magnetic superstrate, good agreement is observed between the CST and the measured results. We note that the feed location had to be slightly adjusted to achieve good matching after using the superstrate due to the loading effect of the superstrate. The overall profile of the structure is only $\lambda_o/7$ where λ_o is the free-space wavelength at the resonance frequency.

The analysis of the MPA covered with engineered superstrate are performed using Intel(R) Core(TM)2 Quad CPU @2.83 GHz machine, the proposed analytical technique requires 6 minutes and 280 megabytes of RAM using MATLAB, while the CST simulations for the same structure requires about 5 hours and 2 gigabytes of RAM when 45 cells/wavelength with total of 2.6 M mesh-cells were used for the entire structure. However, the analytical technique as presented in this work is not capable of determining the input impedance.

We emphasis that the analytical method presented in this paper is not restricted to the case of artificial magnetic superstrate, and can be used for analysis of any superstrate made of engineered structure (positive or negative permeability and/or permittivity) or naturally available material.

V. Conclusions

A fast and accurate analytical technique was developed to calculate the radiation field of an enhanced directivity microstrip antenna covered with an artificial magnetic superstrate. The analytical formulation is based on using the cavity model to replace the patch antenna by two magnetic line sources. Then, the reciprocity theorem and transmission line analogy were used to calculate the far-field of these two magnetic line sources representing the patch antenna. The proposed analytical model was implemented and verified by a comparison with a full-wave simulator for the case of patch antenna covered with different conventional superstrate layers.

As a practical application, the radiation pattern of a patch antenna covered with an artificial magnetic superstrate was calculated using the analytical method. The broadside coupled split ring resonator (SRR) inclusions acting as building blocks for the artificial magnetic superstrate were characterized analytically to obtain its effective permeability and permittivity to be used in the analytical model of the whole radiating system. Measurement results were provided to support the analytical solution. The directivity of the patch antenna covered with the artificial superstrate was improved by about 3.4 dB while maintaining a relatively low profile of the whole structure. The analytical formulation introduced here can be extended for the case of a patch antenna embedded in a multilayered artificial dielectric structure.

Acknowledgment

The authors wish to acknowledge Dr. O. Siddiqui for helping with the experimental part of this work.

References

[1] N. Alexopoulos and D. Jackson, "Fundamental superstrate (cover) effects on printed circuit antennas," *IEEE Trans. Antennas Propag.*, vol. 32, no. 8, pp. 807–816, Aug. 1984.

[2] D. Jackson and N. Alexopoulos, "Gain enhancement methods for printed circuit antennas," *IEEE Trans. Antennas Propag.*, vol. 33, no. 9, pp. 976–987, Sep. 1985.

[3] D. R. Jackson, A. A. Oliner, and A. Ip, "Leaky-wave propagation and radiation for a narrow-beam multiple-layer dielectric structure," *IEEE Trans. Antennas Propag.*, vol. 41, no. 3, pp. 344–348, Mar. 1993.

[4] T. Zhao, D. R. Jackson, J. T. Williams, H. Y. D. Yang, and A. A. Oliner, "2-d periodic leaky-wave antennas-Part I: Metal patch design," *IEEE Trans. Antennas Propag.*, vol. 53, no. 11, pp. 3505–3514, Nov. 2005.

[5] G. Lovat, P. Burghignoli, and D. R. Jackson, "Fundamental properties and optimization of broadside radiation from uniform leaky-wave antennas," *IEEE Trans. Antennas Propag.*, vol. 54, no. 5, pp. 1442–1452, May 2006.

[6] A. Foroozesh and L. Shafai, "Effects of artificial magnetic conductors in the design of low-profile high-gain planar antennas with high-permittivity dielectric superstrate," *IEEE Antenna Wireless Propag. Lett.*, vol. 8, pp. 10–13, 2009.

[7] H. Attia, L. Yousefi, M. M. Bait-Suwailam, M. S. Boybay, and O. M. Ramahi, "Enhanced-gain microstrip antenna using engineered magnetic superstrates," *IEEE Antenna Wireless Propag. Lett.*, vol. 8, pp. 1198–1201, 2009.

[8] A. Foroozesh and L. Shafai, "Investigation into the effects of the patch-type fss superstrate on the high-gain cavity resonance antenna design," *IEEE Trans. Antennas Propag.*, vol. 58, no. 2, pp. 258–270, Feb. 2010.

[9] O. M. Ramahi and Y. T. Lo, "Superstrate effect on the resonant frequency of microstrip antennas," *Microw. Opt. Tech. Lett.*, vol. 5, no. 6, pp. 254–257, Jun. 1992.

[10] W. R. Deal, N. Kaneda, J. Sor, Y. Qian, and T. Itoh, "A new quasi-Yagi antenna for planar active antenna arrays," *IEEE Trans. Microwave Theory Tech.*, vol. 48, no. 6, pp. 910–918, Jun. 2000.

[11] H. Vettikalladi, O. Lafond, and M. Himdi, "High-efficient and high-gain superstrate antenna for 60-GHz indoor communication," *IEEE Antenna Wireless Propag. Lett.*, vol. 8, pp. 1422–1425, 2009.

[12] R. Mittra, Y. Li, and K. Yoo, "A comparative study of directivity enhancement of microstrip patch antennas with using three different superstrates," *Microwave Opt. Tech. Lett.*, vol. 52, no. 2, pp. 327–331, Feb. 2010.

[13] Y. J. Lee, J. Yeo, R. Mittra, and W. S. Park, "Application of electromagnetic bandgap (EBG) superstrates with controllable defects for a class of patch antennas as spatial angular filters," *IEEE Trans. Antennas Propag.*, vol. 53, no. 1, pp. 224–235, Jan. 2005.

[14] H. Attia and O. M. Ramahi, "EBG superstrate for gain and bandwidth enhancement of microstrip array antennas," in *Pro. IEEE AP-S Int. Symp. Antennas Propag.*, San Diego, CA, 2008, pp. 1–4.
[15] H. Attia, L. Yousefi, O. Siddiqui, and O. M. Ramahi, "Analytical formulation of the radiation field of printed antennas in the presence of artificial magnetic superstrates," in *Proc. META'10, the 2nd Int. Conf. on Metamaterials, Photonic Crystals and Plasmonics*, Cairo, Egypt, 2010, pp. 587–591.
[16] A. Foroozesh and L. Shafai, "Size reduction of a microstrip antenna with dielectric superstrate using meta-materials: Artificial magnetic conductors versus magneto-dielectrics," in *Proc. IEEE AP-S Int. Symp. Antennas Propag.*, Albuquerque, NM, Jul. 2006, pp. 11–14.
[17] M. Latrach, H. Rmili, C. Sabatier, E. Seguenot, and S. Toutain, "Design of a new type of metamaterial radome for low frequencies," in *Proc. META08 and NATO Adv. Res. Workshop: Metamater. Secure Inf. Commun. Technol.*, Marrakesh, Morocco, May 2008, pp. 202–211.
[18] X. H. Wu, A. A. Kishk, and A. Glisson, "A transmission line method to compute the far-field radiation of arbitrarily directed hertzian dipoles in a multilayer dielectric structure: Theory and applications," *IEEE Trans. Antennas Propag.*, vol. 54, no. 10, pp. 2731–2741, Oct. 2006.
[19] X. H. Wu, A. A. Kishk, and A. Glisson, "A transmission line method to compute the far-field radiation of arbitrary Hertzian dipoles in a multilayer structure embedded with PEC strip interfaces," *IEEE Trans. Antennas Propag.*, vol. 55, no. 11, pp. 3191–3198, Nov. 2007.
[20] Y. Lo, D. Solomon, and W. Richards, "Theory and experiment on microstrip antennas," *IEEE Trans. Antennas Propag.*, vol. 27, no. 2, pp. 137–145, Mar. 1979.
[21] R. F. Harrington, *Time-Harmonic Electromagnetic Fields*. New York: McGraw-Hill, 1961.
[22] D. M. Pozar, *Microwave Engineering*, 2nd ed. New York: Wiley, 1998.
[23] K. Carver and J. Mink, "Microstrip antenna technology," *IEEE Trans. Antennas Propag.*, vol. 29, no. 1, pp. 2–24, Jan. 1981.
[24] S. Maslovski, P. Ikonen, I. Kolmakov, and S. Tretyakov, "Artificial magnetic materials based on the new magnetic particle: Metasolenoid," *J. Progr. Electromagn. Res. (PIER)*, vol. 54, no. 9, pp. 61–81, Sep. 2005.
[25] K. Buell, H. Mosallaei, and K. Sarabandi, "A substrate for small patch antennas providing tunable miniaturization factors," *IEEE Trans. Antennas Propag.*, vol. 54, no. 1, pp. 135–146, Jan. 2006.

Hussein Attia (S'99) was born in Zagazig, Egypt, in 1977. He received the B.Sc. (highest honors) and M.A.Sc. degrees from Zagazig University, in 1999 and 2006, respectively, both in electronics and communication engineering. He is currently working towards the Ph.D. degree at the University of Waterloo, Waterloo, ON, Canada.

From 1999 to 2006, he was appointed as a lecturer assistant at Zagazig University, where he was involved with teaching, academic advising and research. Since 2007, he has been a teaching assistant and Lecturer (part-time) at the University of Waterloo. His research interests include high-gain handset antennas, analytical techniques for electromagnetic modeling, engineered magnetic metamaterials and electromagnetic interference (EMI).

Mr. Attia is the recipient of a Graduate Scholarship (2007–2010) from Zagazig University.

Leila Yousefi (M'09) was born in Isfahan, Iran, in 1978. She received the B.Sc. and M.Sc. degrees in electrical engineering from Sharif University of Technology, Tehran, Iran, in 2000 and 2003, respectively, and the Ph.D. degree in electrical engineering from the University of Waterloo, Waterloo, ON, Canada, in 2009.

Currently, she is working as a Postdoctoral Fellow at the University of Waterloo. Her research interests include metamaterials, miniaturized antennas, electromagnetic bandgap structures, and MIMO systems.

Omar M. Ramahi (F'09) was born in Jerusalem, Palestine. He received the B.S. degrees in mathematics and electrical and computer engineering (*summa cum laude*) from Oregon State University, Corvallis, and the M.S. and Ph.D. degrees in electrical and computer engineering from the University of Illinois at Urbana-Champaign.

He held a visiting fellowship position at the University of Illinois at Urbana-Champaign and then worked at Digital Equipment Corporation (presently, HP), where he was a member of the alpha server product development group. In 2000, he joined the faculty of the James Clark School of Engineering, University of Maryland at College Park, as an Assistant Professor, a tenured Associate Professor, and was also a faculty member of the CALCE Electronic Products and Systems Center. Presently, he is a Professor in the Electrical and Computer Engineering Department and holds the NSERC/RIM Industrial Research Associate Chair, University of Waterloo, Ontario, Canada. He holds cross appointments with the Department of Mechanical and Mechatronics Engineering and the Department of Physics and Astronomy. He has authored and coauthored over 240 journal and conference papers. He is a coauthor of the book *EMI/EMC Computational Modeling Handbook* (Springer-Verlag, 2001, 2nd ed.).

Dr. Ramahi serves as an Associate Editor for the IEEE TRANSACTIONS ON ADVANCED PACKAGING and as the IEEE EMC Society Distinguished Lecturer.